Translocon component Sec62 acts in endoplasmic reticulum turnover during stress recovery — Source link ⬈

Fiorenza Fumagalli, Fiorenza Fumagalli, Julia Noack, Timothy J. Bergmann ...+26 more authors

Institutions: University of Bern, University of Lugano, École Polytechnique Fédérale de Lausanne, Saarland University ...+3 more institutions

Topics: Unfolded protein response, Endoplasmic reticulum, Translocon, Reticulophagy and SEC62

Related papers:

- Regulation of endoplasmic reticulum turnover by selective autophagy

- Full length RTN3 regulates turnover of tubular endoplasmic reticulum via selective autophagy

- CCPG1 Is a Non-canonical Autophagy Cargo Receptor Essential for ER-Phagy and Pancreatic ER Proteostasis.

- Receptor-mediated selective autophagy degrades the endoplasmic reticulum and the nucleus

- ATL3 Is a Tubular ER-Phagy Receptor for GABARAP-Mediated Selective Autophagy.

Year: 2016

Translocon component Sec62 acts in endoplasmic reticulum turnover during stress recovery

Fumagalli, Fiorenza ; Noack, Julia ; Bergmann, Timothy J ; Presmanes, Eduardo Cebollero ; Pisoni, Giorgia Brambilla ; Fasana, Elisa ; Fregno, Ilaria ; Galli, Carmela ; Loi, Marisa ; Solda, Tatiana ; D'Antuono, Rocco ; Raimondi, Andrea ; Jung, Martin ; Melnyk, Armin ; Schorr, Stefan ; Schreiber, Anne ; Simonelli, Luca ; Varani, Luca ; Wilson-Zbinden, Caroline ; Zerbe, Oliver ; Hofmann, Kay ; Peter, Matthias ; Quadroni, Manfredo ; Zimmermann, Richard ; Molinari, Maurizio

Abstract: The endoplasmic reticulum (ER) is a site of protein biogenesis in eukaryotic cells. Perturbing ER homeostasis activates stress programs collectively called the unfolded protein response (UPR). The UPR enhances production of ER-resident chaperones and enzymes to reduce the burden of misfolded proteins. On resolution of ER stress, ill-defined, selective autophagic programs remove excess ER components. Here we identify Sec62, a constituent of the translocon complex regulating protein import in the mammalian ER, as an ER-resident autophagy receptor. Sec62 intervenes during recovery from ER stress to selectively deliver ER components to the autolysosomal system for clearance in a series of events that we name recovER-phagy. Sec62 contains a conserved LC3-interacting region in the C-terminal cytosolic domain that is required for its function in recovER-phagy, but is dispensable for its function in the protein translocation machinery. Our results identify Sec62 as a critical molecular component in maintenance and recovery of ER homeostasis.

Sec62 regulates endoplasmic reticulum turnover during recovery from ER stress

Fiorenza Fumagalli[1,2,3†], Julia Noack[1,2†], Timothy J. Bergmann[1,2,4†], Eduardo Cebollero[1,2†], Giorgia Brambilla Pisoni[1,2,4], Elisa Fasana[1,2], Ilaria Fregno[1,2,4], Carmela Galli[1,2], Marisa Loi[1,2], Tatiana Soldà[1,2], Rocco D'Antuono[1,2], Andrea Raimondi[5], Martin Jung[6], Armin Melnyk[6], Stefan Schorr[6], Anne Schreiber[7], Luca Simonelli[1,2], Luca Varani[1,2], Caroline Wilson-Zbinden[7], Oliver Zerbe[8], Kay Hofmann[9], Matthias Peter[7], Manfredo Quadroni[10], Richard Zimmermann[6] and Maurizio Molinari[1,2,11*]

[1]Università della Svizzera italiana, CH-6900 Lugano, Switzerland
[2]Institute for Research in Biomedicine, CH-6500 Bellinzona, Switzerland
[3]Graduate School for Cellular and Biomedical Sciences, University of Bern, CH-3000 Bern, Switzerland
[4]ETH Zurich, D-BIOL, CH-8093 Zurich, Switzerland
[5]Experimental Imaging Center, San Raffaele Scientific Institute, I-20132 Milan, Italy
[6]Medical Biochemistry and Molecular Biology, Saarland University, D-66421 Homburg, Germany
[7]Department of Biology, Institute of Biochemistry, Swiss Federal Institute of Technology, CH-8093 Zurich, Switzerland
[8]Department of Chemistry, University of Zurich, CH-8057 Zurich, Switzerland
[9]Institute for Genetics, University of Cologne, D-50674 Cologne, Germany
[10]Center for Integrative Genomics, University of Lausanne, CH-1015 Lausanne, Switzerland
[11]Ecole Polytechnique Fédérale de Lausanne, School of Life Sciences, CH-1015 Lausanne, Switzerland

Correspondence to: maurizio.molinari@irb.usi.ch

†Equal Contributors

The endoplasmic reticulum (ER) is a site of protein biogenesis in eukaryotic cells. Perturbing ER homeostasis activates stress programs collectively called the unfolded protein response (UPR). The UPR enhances production of ER-resident chaperones and enzymes to reduce the burden of misfolded proteins [1]. Upon resolution of ER stress, excess ER components are removed by ill-defined, selective autophagic programs [2-4]. Here, using biochemical and cell-based assays, we identify Sec62, a constituent of the translocon complex that regulates protein import in the mammalian ER, as an ER-resident autophagy receptor. The newly discovered function of Sec62 is enhanced during recovery from ER stress to selectively deliver ER components to the autolysosomal system for clearance. Sec62 contains a conserved LC3-interacting region (LIR) in the C-terminal cytosolic domain that is required for its function in ER turnover, but dispensable for its function in the protein translocation machinery. Quantitative mass spectrometry analyses [5] of autolysosomal fractions upon selective inactivation of the Sec62-regulated ER clearance inform on the selectivity of Sec62-regulated ER-phagy. Taken together, our results identify Sec62 as a critical molecular component in maintenance and recovery of ER homeostasis, launching molecular dissection of selective ER turnover in health and disease [2-4].

To define mechanisms that regulate the return of ER-resident chaperones and folding factors to their physiologic intracellular level after resolution of an ER stress, we established a protocol for reversible induction of UPR in cultured mammalian cells (**Fig. 1a**). Briefly, human embryonic kidney cells (HEK293) or mouse embryonic fibroblasts (MEF) were exposed for 12 h to non-toxic doses of cyclopiazonic acid (CPA), a reversible inhibitor of the sarco/endoplasmic reticulum calcium pump [6]. The return of ER-resident gene products at their pre-stress level was monitored during resolution of the UPR obtained upon CPA wash out (**Fig. 1b-f** and **Extended data Fig. 1** for other ER stress inducers).

Consistent with UPR induction, cell treatment with CPA caused splicing of Xbp1 transcripts (**Extended data Fig. 2a**), 25% attenuation of global protein synthesis (**Extended data Fig. 2b, d**), induction of select ER stress marker transcripts (**Fig. 1b**) and proteins (**Fig. 1c-f**, **Extended data Fig. 2c-f**). CPA wash out initiated a recovery phase characterized by the rapid return of ER stress-induced transcripts at, or below, their pre-stress levels (**Fig. 1b**, recovery, $T_{1/2 \ average} \approx 1$ h, blue line). The corresponding ER stress-induced proteins returned to their physiologic levels with much slower kinetics (**Fig. 1c, d**, $T_{1/2 \ average} \approx 10$ h, blue).

With the exception of Herp, which is rapidly turned over with intervention of proteasomes (**Fig. 1c, d**, **Extended data Fig. 2e, f**, $T_{1/2} < 2$ h, red lines and not further investigated in this work), return of ER stress-induced proteins to their pre-stress, physiologic level was blocked by the lysosomotropic and autophagy inhibitor bafilomycin A1 (BafA1 [7], **Fig. 1e, f** and **Extended data Fig. 2f**). Immunofluorescence (IF) analyses revealed that BafA1 treatment during recovery from ER stress caused accumulation of Cnx (**Fig. 1g, 2a**) and other membrane and luminal ER marker proteins such as Sec62 and Crt (**Fig. 2b** and **Extended data Fig. 3**) in 0.5-1.5 µm diameter cytoplasmic puncta that rapidly disappeared upon BafA1 wash out (**Extended data Fig. 4**). Cytosolic puncta containing ER marker proteins were significantly less abundant when incubation with BafA1 was performed in unstressed cells or during CPA treatment (**Fig. 1h, i**). ER puncta co-localize with GFP-LC3 and are surrounded by GFP-Rab7 and endogenous Lamp1, three marker proteins of autolysosomes that accumulate with their un-degraded content upon inhibition of lysosomal activity with BafA1 [7] (**Fig. 2a**, **b, Extended data Fig. 3, 5**). These data were confirmed by correlative light-electron microscopy (CLEM, **Fig. 2c**) and immuno-electron microscopy (**Fig. 2d**). Consistent with an intervention of the autophagy machinery for ER turnover during recovery from ER stress, ER marker proteins were not delivered to autolysosomes (**Fig. 2e-i**) and showed delayed return to their pre-stress levels (**Extended data Fig. 2g**) in cells lacking the autophagy proteins Atg7 or Atg5.

Selective removal of excess ER during recovery from ER stress would require an autophagy receptor at its membrane. LC3-interacting regions (LIR) of autophagy receptors recruit LC3-II, the form of LC3 anchored to the membrane of a phagophore, as an initial step in selective autophagy [8]. A bioinformatic analysis in search for novel autophagy receptors revealed the presence of a conserved LIR motif in the C-terminal cytosolic domain of Sec62 (-NDFEMIT-, residues 361-367 of human Sec62, **Extended data Fig. 6a, b**). Sec62 is an ER-resident protein with a well-established role in post-translational protein import in the ER that obligatorily depends on formation of Sec62:Sec63 heterodimeric complexes in association with the Sec61 translocon [9,10]. The LIR motif of Sec62 adapts to the LC3 protein-binding groove establishing specific contacts according to docking and molecular dynamics simulations (**Fig. 3a**) and binds to LC3B *in vitro* as determined by SPR **(Fig. 3b)**, NMR **(Fig. 3d)** and peptide array analyses **(Extended data Fig. 6c)**. Mutation of the -FEMI- sequence in the Sec62 LIR with -AAAA- abolished these interactions **(Fig. 3c, e and Extended data Fig.**

6c). Consistent with *in silico* and *in vitro* data, the immunoisolation of endogenous (**Extended data Fig. 7a**, lane 5) and ectopically expressed Sec62 (**Fig. 3f**, lanes 3 *vs.* 4, **Extended data Fig. 7b**, lanes 3 *vs.* 4) revealed the LIR-dependent association with endogenous LC3-II in living cells, which was stabilized with BafA1 (**Extended data Fig. 7a**, lanes 4 vs. *5*). The association between endogenous Sec62 and LC3-II did not require Sec63 (**Extended data Fig. 7c**, right panel, lane 8) and was recapitulated by appending the cytosolic LIR-containing domain of Sec62 to ER membrane anchored GFP (GFP$_{TM}$62, **Fig. 3f**, lane 8). For all proteins tested, association with endogenous and recombinant LC3 was abolished upon mutation of the Sec62 LIR (**Fig. 3f**, lanes 4, 9, 11, **Extended data Fig. 7b**, lane 4, **7c**, lane 7) and in ATG7 KO MEF with inactive autophagy (**Fig. 3f**, lanes 5, 10, 11).

Consistent with a role of Sec62 in autophagy-regulated recovery from ER stress, silencing of Sec62 expression in MEF (**Fig. 4a**, lower panel, **b**), or KO of Sec62 obtained in HEK293 cells with CRISPR/Cas9 technology (**Fig. 4c** and **Extended data Fig. 8**) inhibited delivery of ER protein markers to autolysosomes during recovery from ER stress as shown by the LAMP1-positive vesicles devoid of ER marker proteins (**Fig. 4a**, lower panel, **4c, Extended data Fig. 8e**). Induction of Sec62 expression (**Extended data Fig. 8b**) re-established delivery of ER markers to autolysosomes in CRISPR62 cells (**Fig. 4d**), whereas the induction of Sec62LIRmut did not (**Fig. 4e**). The KO of Sec62 also delayed return of excess ER marker proteins to pre-stress levels upon conclusion of the CPA-induced ER stress (**Extended data Fig. 8h**).

Overexpression of Sec62 (**Fig. 4f**) or of a GFP$_{TM}$62 chimera that displays the C-terminal cytosolic LIR domain of Sec62 on ER membrane-bound GFP (**Extended data Fig. 9a, c**, +BafA1) triggered delivery of ER protein markers to autolysosomes in unstressed cells thus reducing their intracellular level (**Extended data Fig. 8i**). This was not observed upon overexpression of Sec62LIRmut or GFP$_{TM}$62LIRmut that display inactive LIR domains (**Fig. 4g**, **Extended data Fig. 9b, d**, +BafA1). Aberrant delivery of ER portions to autolysosomes at steady state did also occur upon KO of Sec63 (**Extended data Fig. 8f**). Altogether, these data show that the LIR motif of Sec62 is required and sufficient for delivery of ER portions to autolysosomes and that in contrast to its role in protein translocation [9,10] (**Fig. 4h and Extended data Fig. 10**), the role of Sec62 in ER turnover during recovery from ER stress does not require Sec63. Separation of the roles of Sec62 in protein translocation and in removal of excess ER during recovery from ER stress was confirmed by *in vivo* protein

translocation experiments [9], where the Sec62LIRmut, which is inactive in recovery from ER stress, was equally effective as ectopic Sec62 in complementing the KO and the silencing of endogenous Sec62 (**Fig. 4h, lanes 9 and 10, Extended data Fig. 10**).

Next, we exploited the fact that Sec62LIRmut overexpression inhibits delivery of excess ER marker proteins to autolysosomes, to identify the proteins cleared from cells in a Sec62-regulated pathway. To address this, we enriched autolysosomal vesicles (AV) accumulating in HEK293 cells with inducible expression of Sec62 or Sec62LIRmut (Flp Sec62 and Flp Sec62LIRmut) recovering from a CPA-induced ER stress and exposed to BafA1 in isopycnic density gradients. In such gradients, AV protein markers such as endogenous LC3-II and p62/Sequestosome float from the loading region of the isopycnic gradients (L, fraction 12) to the lightest fraction 1 at the top (AV, **Extended data Fig. 11a** and lowest panels in **Fig. 4i**) [11]. Expression of the Sec62LIRmut did not significantly affect the generation of AV as demonstrated by the unchanged floatation of AV marker proteins (two lowest panels in **Fig. 4i**) and the unchanged number of GFP-LC3-/p62-positive autophagosomes as determined in IF (**Extended data Fig. 11b**). Rather, it substantially depleted AV fractions of select ER protein markers (**Fig. 4i**, fraction 1, Flp Sec62 *vs.* Flp Sec62LIRmut). Hampered ER marker protein floatation also occurred in cells where formation of autolysosomes is defective upon Atg7 KO (**Extended data Fig. 11c**).

Mass Spectrometry-based Label Free quantitation (MS-LFQ [5]) of the proteins contained in the lightest (AV) fraction of the isopycnic gradient derived from cells expressing Sec62 or the Sec62LIRmut failed to reveal significant differences for bulk autophagy marker proteins such as LC3, Lamp1, Rab7, p62/Sequestosome and many others, where negative values (**Fig. 4j**), resp. values below the diagonal (**Extended data Fig. 12**), would indicate depletion of protein markers from AV upon expression of the Sec62LIRmut. Rather, the MS-LFQ analyses confirmed the depletion of select ER markers such as general chaperones (e.g., BiP, Cnx, Crt, Grp94), and protein disulfide isomerase family members (PDI) from the AV (**Fig. 4j** and **Extended data Fig. 12**). In contrast, expression of the Sec62LIRmut did not affect formation of bulk autophagosomes (see above) or the delivery to autolysosomes of most mitochondrial or most ERAD protein markers (**Fig. 4j** and **Extended data Fig. 12**). Altogether, these data establish a *novel* role of Sec62 in controlling ER homeostasis by promoting delivery of select ER components to the autophagic pathway during resolution of ER stress.

The Sec61 translocon is a highly dynamic protein-conducting channel whose composition is regulated in an ill-defined manner to determine the efficiency and the quantity of membrane and secretory protein entrance into the secretory pathway [10]. Here we show that one of its components, Sec62, is an ER-phagy receptor that delivers ER portions to the autolysosomal pathway for turnover. This novel role of Sec62 in ER physiology is enhanced after successful resolution of ER stress, contribute to re-establish pre-stress ER homeostasis and opens several lines of research aiming at better understanding of how mammalian cells maintain or re-establish proteostasis. The activity of Sec62 in translocation of nascent proteins across the ER membrane is carried out in complex with Sec63 and requires formation of higher order complexes with other components of the Sec61 translocon [9,10,12-15]. However, ectopic expression of Sec62 or of reporter proteins displaying its LIR containing cytosolic domain is sufficient to enhance delivery of ER protein markers to the autolysosomal system for clearance, and Sec63 is not required for Sec62 function in ER stress recovery. This supports a role of Sec62 as an ER-phagy receptor, which is fully independent of its *conventional* role in the translocation machinery. Since Sec62 is not induced upon ER stress, it will be of interest to establish whether the employment of Sec62 as ER-phagy receptor requires disassembly of functional translocons (our tests do not reveal impairment of ERj3 translocation during cell recovery from ER stress, **Fig. 4h**, lane 3 *vs.* 1) or whether the Sec62 regulating delivery of excess ER to autolysosomes during recovery from ER stress is recruited from a different pool of cellular protein. Cumulating evidences identify SEC62 as a candidate oncogene, which is frequently amplified in non-small cell lung, prostate, thyroid cancers correlating with reduced patient survival, higher metastatic and invasive potential and higher ER stress tolerance [16-18]. In contrast, the other components of the Sec61 translocation machinery show invariant expression in the same diseases, speaking for an *individual* involvement of Sec62 in cancer promotion and pathogenesis highlighting Sec62 and, possibly, its role in ER-phagy as a potential target for anti-cancer therapy. An important issue to be addressed in further studies is the selectivity of the Sec62-regulated ER delivery to autolysosomes. Here we just grasp the surface by reporting that highly induced (e.g., BiP, Crt, several oxidoreductases), modestly induced (Cnx) and non-induced proteins (e.g., Tmx1 [19]) are delivered to autolysosomes during recovery from ER stress, whereas, as one example, most ERAD factors are not (**Fig. 4j**). This might reflect the sub-organellar compartmentalization of ER activities. Other issues to be addressed in future studies are whether Sec62 involvement in recovery from ER stress also extends to the clearance of Ire1 and/or PERK foci [20] that would otherwise maintain the ER stress status (note that Ire1 was identified as one of the cargo of the Sec62-dependent

protein delivery to autolysosomes, **Fig. 4i**), the putative role of Sec62-driven ER-phagy in clearance of proteasome- or retrotranslocation-resistant misfolded polypeptides that may accumulate in ER subdomains, and a possible crosstalk of Sec62 with Fam134 family members that have recently been proposed to maintain ER homeostasis at steady state [21].

References

1   Walter, P. & Ron, D. The unfolded protein response: from stress pathway to homeostatic regulation. *Science* **334**, 1081-1086, doi:10.1126/science.1209038 (2011).

2   Federovitch, C. M., Ron, D. & Hampton, R. Y. The dynamic ER: experimental approaches and current questions. *Curr Opin Cell Biol* **17**, 409-414, doi:10.1016/j.ceb.2005.06.010 (2005).

3   Bolender, R. P. & Weibel, E. R. A morphometric study of the removal of phenobarbital-induced membranes from hepatocytes after cessation of treatment. *J Cell Biol* **56**, 746-761 (1973).

4   Feldman, D., Swarm, R. L. & Becker, J. Elimination of excess smooth endoplasmic reticulum after phenobarbital administration. *J Histochem Cytochem* **28**, 997-1006 (1980).

5   Cox, J. *et al.* Accurate Proteome-wide Label-free Quantification by Delayed Normalization and Maximal Peptide Ratio Extraction, Termed MaxLFQ. *Mol Cell Proteomics* **13**, 2513-2526, doi:10.1074/mcp.M113.031591 (2014).

6   Pirot, P. *et al.* Global profiling of genes modified by endoplasmic reticulum stress in pancreatic beta cells reveals the early degradation of insulin mRNAs. *Diabetologia* **50**, 1006-1014, doi:10.1007/s00125-007-0609-0 (2007).

7   Klionsky, D. J., Elazar, Z., Seglen, P. O. & Rubinsztein, D. C. Does bafilomycin A(1) block the fusion of autophagosomes with lysosomes? *Autophagy* **4**, 849-850 (2008).

8   Birgisdottir, A. B., Lamark, T. & Johansen, T. The LIR motif - crucial for selective autophagy. *J Cell Sci* **126**, 3237-3247, doi:10.1242/jcs.126128 (2013).

9   Lang, S. *et al.* Different effects of Sec61 alpha, Sec62 and Sec63 depletion on transport of polypeptides into the endoplasmic reticulum of mammalian cells. *J Cell Sci* **125**, 1958-1969, doi:10.1242/jcs.096727 (2012).

10   Conti, B. J., Devaraneni, P. K., Yang, Z. Y., David, L. L. & Skach, W. R. Cotranslational Stabilization of Sec62/63 within the ER Sec61 Translocon Is Controlled by Distinct Substrate-Driven Translocation Events. *Mol Cell* **58**, 269-283, doi:10.1016/j.molcel.2015.02.018 (2015).

11   Klionsky, D. J. *et al.* Guidelines for the use and interpretation of assays for monitoring autophagy. *Autophagy* **8**, 445-544 (2012).

12   Johnson, N. *et al.* The Signal Sequence Influences Post-Translational ER Translocation at Distinct Stages. *PLoS One* **8**, doi:10.1371/journal.pone.0075394 (2013).

13   Lakkaraju, A. K. K. *et al.* Efficient secretion of small proteins in mammalian cells relies on Sec62-dependent posttranslational translocation. *Mol Biol Cell* **23**, 2712-2722, doi:10.1091/mbc.E12-03-0228 (2012).

14   Wang, X. & Johnsson, N. Protein kinase CK2 phosphorylates Sec63p to stimulate the assembly of the endoplasmic reticulum protein translocation apparatus. *J Cell Sci* **118**, 723-732, doi:10.1242/jcs.01671 (2005).

15   Meyer, H. A. *et al.* Mammalian Sec61 is associated with Sec62 and Sec63. *J Biol Chem* **275**, 14550-14557 (2000).

16   Linxweiler, M. *et al.* Sec62 Bridges the Gap from 3q Amplification to Molecular Cell Biology in Non-Small Cell Lung Cancer. *Am J Pathol* **180**, 473-483, doi:10.1016/j.ajpath.2011.10.039 (2012).

17   Greiner, M. *et al.* Silencing of the SEC62 gene inhibits migratory and invasive potential of various tumor cells. *Int J Cancer* **128**, 2284-2295, doi:10.1002/ijc.25580 (2011).

18   Jung, V. *et al.* Genomic and expression analysis of the 3q25-q26 amplification unit reveals TLOC1/SEC62 as a probable target gene in prostate cancer. *Mol Cancer Res* **4**, 169-176 (2006).

19   Pisoni, G. B., Ruddock, L. W., Bulleid, N. & Molinari, M. Division of labor among oxidoreductases: TMX1 preferentially acts on transmembrane polypeptides. *Mol Biol Cell* **26**, 3390-3400, doi:10.1091/mbc.E15-05-0321 (2015).

20   Li, H., Korennykh, A. V., Behrman, S. L. & Walter, P. Mammalian endoplasmic reticulum stress sensor IRE1 signals by dynamic clustering. *P Natl Acad Sci USA* **107**, 16113-16118, doi:10.1073/pnas.1010580107 (2010).

21   Khaminets, A. *et al.* Regulation of endoplasmic reticulum turnover by selective autophagy. *Nature* **522**, 354-358, doi:10.1038/nature14498 (2015).

22   Schindelin, J. *et al.* Fiji: an open-source platform for biological-image analysis. *Nat Methods* **9**, 676-682, doi:10.1038/NMETH.2019 (2012).

23   Carpenter, A. E. *et al.* CellProfiler: image analysis software for identifying and quantifying cell phenotypes. *Genome Biol* **7**, doi:10.1186/Gb-2006-7-10-R100 (2006).

24   Mizushima, N., Ohsumi, Y. & Yoshimori, T. Autophagosome formation in mammalian cells. *Cell Struct Funct* **27**, 421-429.

25   Soding, J. Protein homology detection by HMM-HMM comparison. *Bioinformatics* **21**, 951-960, doi:10.1093/bioinformatics/bti125 (2005).

26   Raveh, B., London, N. & Schueler-Furman, O. Sub-angstrom modeling of complexes between flexible peptides and globular proteins. *Proteins* **78**, 2029-2040, doi:10.1002/prot.22716 (2010).

27   London, N., Raveh, B., Cohen, E., Fathi, G. & Schueler-Furman, O. Rosetta FlexPepDock web server-high resolution modeling of peptide-protein interactions. *Nucleic Acids Res* **39**, W249-W253, doi:10.1093/nar/gkr431 (2011).

28   Hilpert, K., Winkler, D. F. H. & Hancock, R. E. W. Peptide arrays on cellulose support: SPOT synthesis, a time and cost efficient method for synthesis of large numbers of peptides in a parallel and addressable fashion. *Nat Protoc* **2**, 1333-1349, doi:10.1038/nprot.2007.160 (2007).

29   Wilm, M. *et al.* Femtomole sequencing of proteins from polyacrylamide gels by nano-electrospray mass spectrometry. *Nature* **379**, 466-469.

30   Cox, J. & Mann, M. 1D and 2D annotation enrichment: a statistical method integrating quantitative proteomics with complementary high-throughput data. *BMC Bioinformatics* **13**, doi:10.1186/1471-2105-13-S16-S12 (2012).

31   Vizcaino, J. A. *et al.* 2016 update of the PRIDE database and its related tools. *Nucleic Acids Res* **44**, D447-D456, doi:10.1093/nar/gkv1145 (2016).

Author contribution

F.F. and J.N. performed biochemical and transcriptional analyses, IF, image quantifications, MS analysis; T.J.B. analyzed protein associations in living cells, performed qPCRs, analyzed MS data; G.B.P. and E.C. prepared DNA constructs, performed initial biochemical analyses; E.F. performed IF and analysis of MS and biochemical data; I.F. performed biochemical analysis, toxicity assays and analysis of MS data; C.G. prepared plasmids for Sec62 and Sec62LIRmut expression, generated and characterized inducible cell lines, performed and analyzed isopycnic density gradients; M.L. performed and analyzed isopycnic density gradients, MS data, contributed to the generation of the FlipIn T-rex CRISPR62 and CRISPR63 cell lines; T.S. generated and characterized the FlipIn T-rex CRISPR62 and CRISPR63 cell lines; R.D'A. developed CellProfiler pipelines; L.S. and L.V. designed and performed computational simulations and structural analysis; A.R. CLEM and electron microscopy on murine cell lines; M.J. and A.M. synthesized peptides and used them in LC3 interaction analysis; S.S. carried out protein transport into the ER in living cells. A.S.; C.W.-Z.; O.Z. performed NMR experiments and analyzed data; M.P.; K.H. performed the bioinformatic analyses to identify the Sec62 LIR; M.Q. carried out mass spectrometry measurements, protein identification and quantification on autolysosome fractions; R.Z. Supervised protein transport and peptide binding experiments and was involved in writing of the manuscript; M.M. designed the study, analyzed data and wrote the manuscript. All the authors discussed the results and the manuscript.
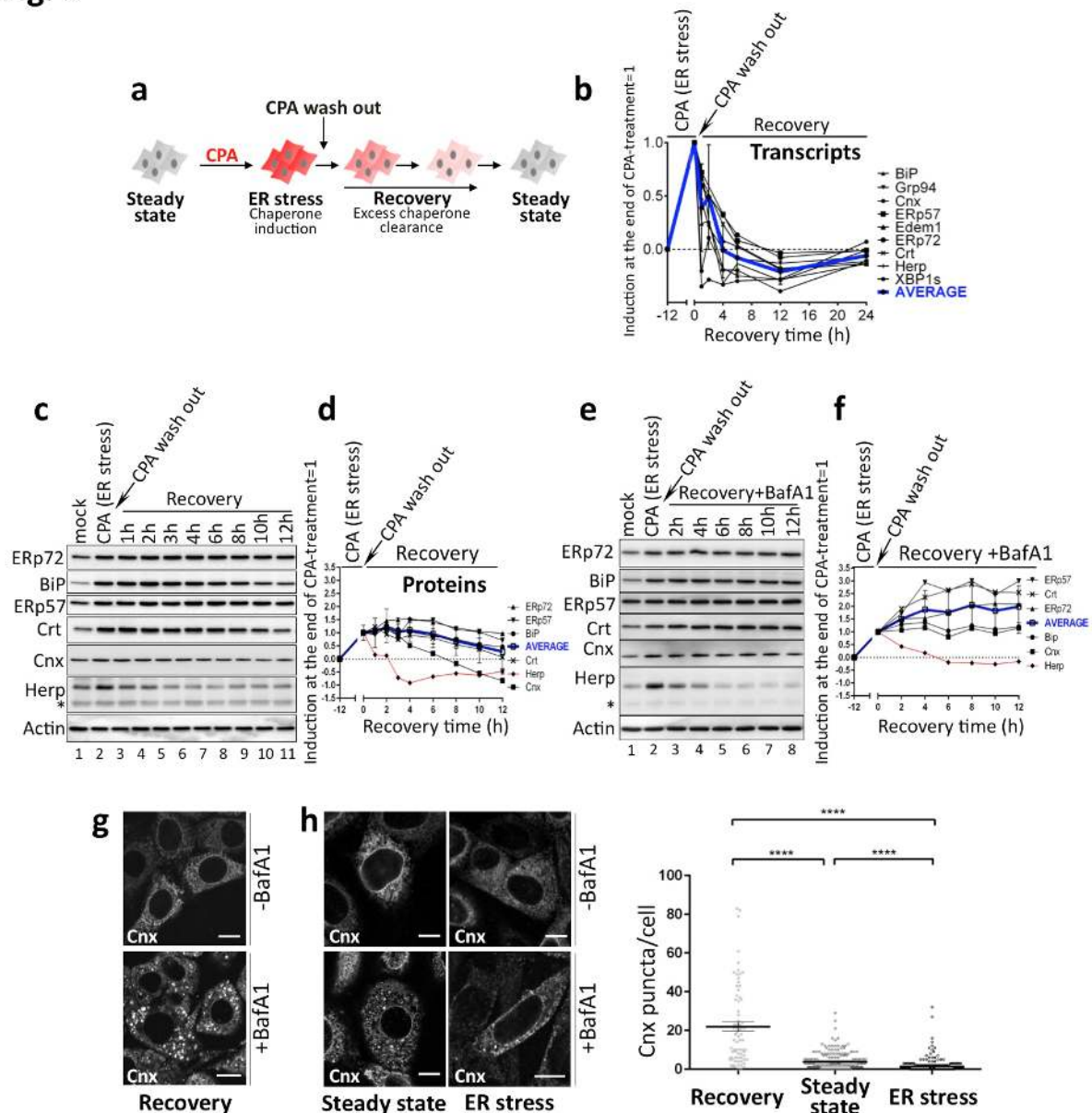
Fig. 1. Measuring transient ER stress and post stress ER recovery. (**a**) Experimental scheme. MEF or HEK293 cells treated with an ER stress-inducing drug (e.g., 10-30 µM CPA) for 12 h. CPA is washed out and cells are grown in normal cell culture media (recovery phase). (**b**) Measuring selected ER gene transcripts with quantitative real time PCR during ER stress and during recovery after CPA wash out. (**c**) Select experiment showing the fluctuation of ER marker proteins monitored by WB during CPA-induced ER stress and during 1-12 h after CPA wash out (Recovery). (**d**) Quantification of (c) **Mean of at least two independent**. Average: mean of values for all proteins except HERP (**e**) Same as (c) in cells exposed to BafA1 during recovery. (**f**) Quantification of (e). n=1, except for the 12 h, where n=2 (mean shown). Average: mean of values for all proteins except HERP. (**g**) Intracellular

distribution of Cnx during recovery from ER stress in untreated cells (-BafA1) and in cells incubated for 3 h with BafA1 (+BafA1). Comparison of ER marker proteins distribution in untreated and BafA1-treated cells is also shown in **Extended Fig. 3**. (**h**) Same as (g) at steady state and during cell exposure to CPA (ER stress). Scale bars: 10 µm. (**i**) Cnx puncta (panels g, h) were quantified with the CellProfiler software. Each dot in the graph represents one cell n = 73, 215, 269 for recovery, steady state and stress, respectively. Bar=mean. **** $p < 0.0001$, t-test.
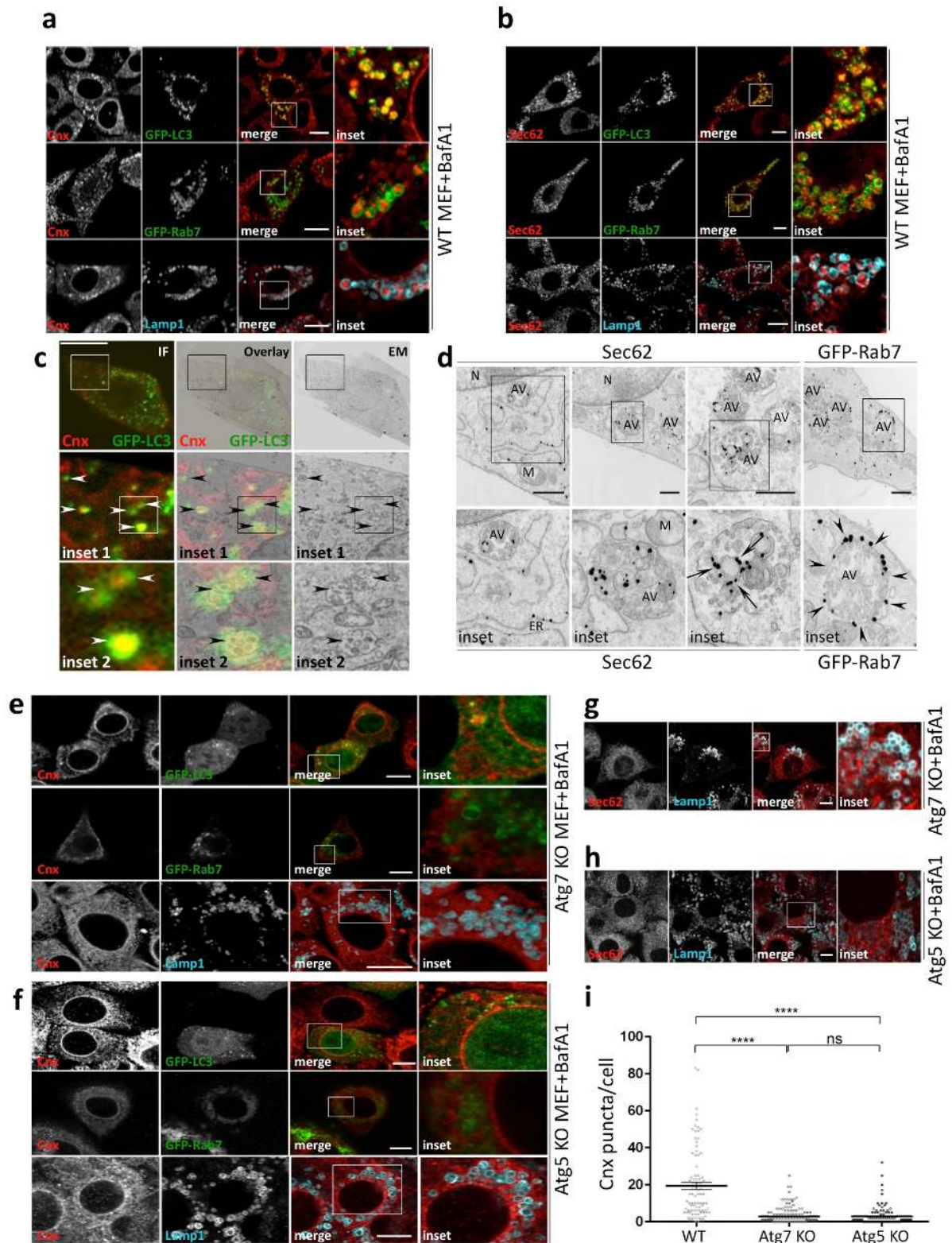
Fig. 2. Intracellular accumulation of ER marker proteins upon inhibition of ER stress recovery. (a) Upon inhibition of ER stress recovery in MEF cells, Cnx co-localizes with GFP-LC3 (upper panels), in structures surrounded by GFP-Rab7 (middle) and endogenous

Lamp1 (lower). (**b**) Same as (a) for another ER protein marker, Sec62. Other examples are shown in **Extended data Fig. 3**. (**c**) CLEM. The co-localization of GFP-LC3 and Cnx was monitored by confocal IF. Serial sections of the selected cells were further processed and analyzed by EM. Arrowheads indicate vesicular structures in which GFP-LC3 and Cnx co-localize. Scale bar: 10 μm. (**d**) Ultrastructural characterization of ER-containing autolysosomes by immunoelectron microscopy. Sec62 and GFP-Rab7 are shown. AV: autophagic vesicles with Sec62-positive ER fragments (arrows) and Rab7 in the limiting membrane (arrowheads); M: mitochondria; N: nucleus; ER: endoplasmic reticulum. Scale bar: 1 μm. (**e**) Same as (a) in Atg7 KO MEF. (**f**) Same as (a) in Atg5 KO MEF. (**g**) Same as (b) in Atg7 KO MEF. (**h**) Same as (b) in Atg5 KO MEF. Scale bars: 10 μm. (**i**) Quantification as in (Fig. 1i). n = 90, 170 and 116 for WT, ATG7 and ATG5 KO, respectively. **Bar=mean.** **** $p < 0.0001$, t-test.
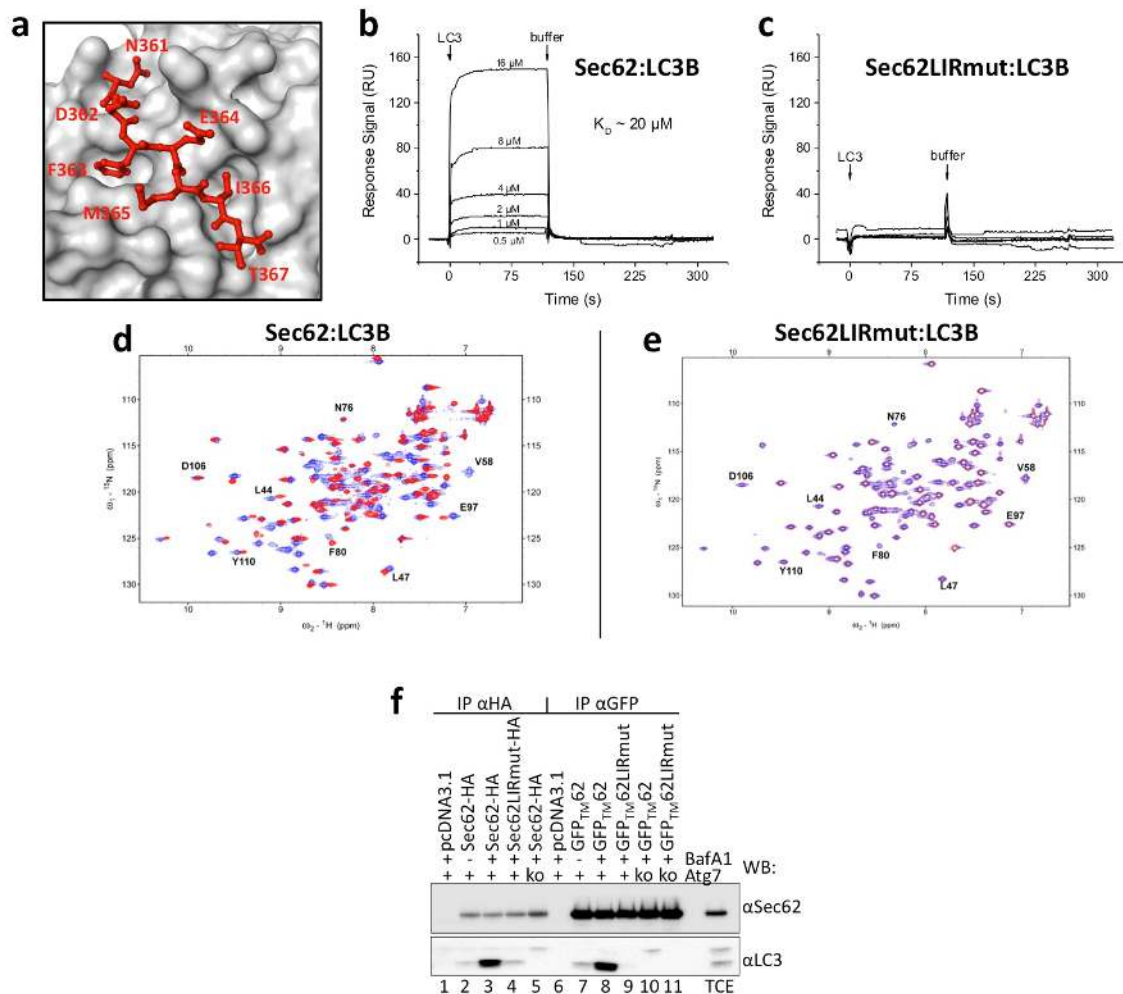
Fig. 3. (**a**) The Sec62 LIR (red sticks) adapts to the LC3 protein-binding groove (grey surface) establishing specific contacts according to docking and molecular dynamics simulations. Intermolecular electrostatic interactions are present along the walls of the LC3 binding pocket. LC3 hydrophobic cavities are filled by F363 and I366. (**b,c**) Comparison of LC3 binding to WT (biotin-352-KSQHSSGNGND**FEMI**TKEE-370 of human Sec62) and LIRmut (biotin-352-KSQHSSGNGND**AAAA**TKEE-370) peptides by SPR. LC3 only binds to the WT peptide with an affinity of approximately 20 µM. (**d, e**) Probing the interaction between LC3 and WT (357-SGNGND**FEMI**TKEE-370) or LIRmut (357-SGNGND**AAAA**TKEE-370) peptides by solution NMR spectroscopy. [^{15}N,^{1}H]-HSQC spectra of uniformly ^{15}N-labeled LC3 (free, blue) in complex with unlabeled WT peptide (panel d, red) or LIRmut (panel e, red). The NMR signal of some LC3 residues changes upon addition of the WT peptide, indicating an interaction. There are no changes, hence

14

interaction, with the LIRmut. The peaks of selected LC3 residues are labeled. (**f**) MEF (Atg7 KO are shown with ko) mock transfected (pcDNA3.1), transfected for expression of Sec62, Sec62LIRmut, GFP$_{TM}$62 or GFP$_{TM}$62LIR, treated (+) or not (-) with BafA1. Complexes stabilized with DSP were immunoisolated from lysates with anti-HA (lanes 1-5) or anti-GFP (lanes 6-11) to visualize association of endogenous LC3-II in WB. TCE, total cell extract.

Fig 4
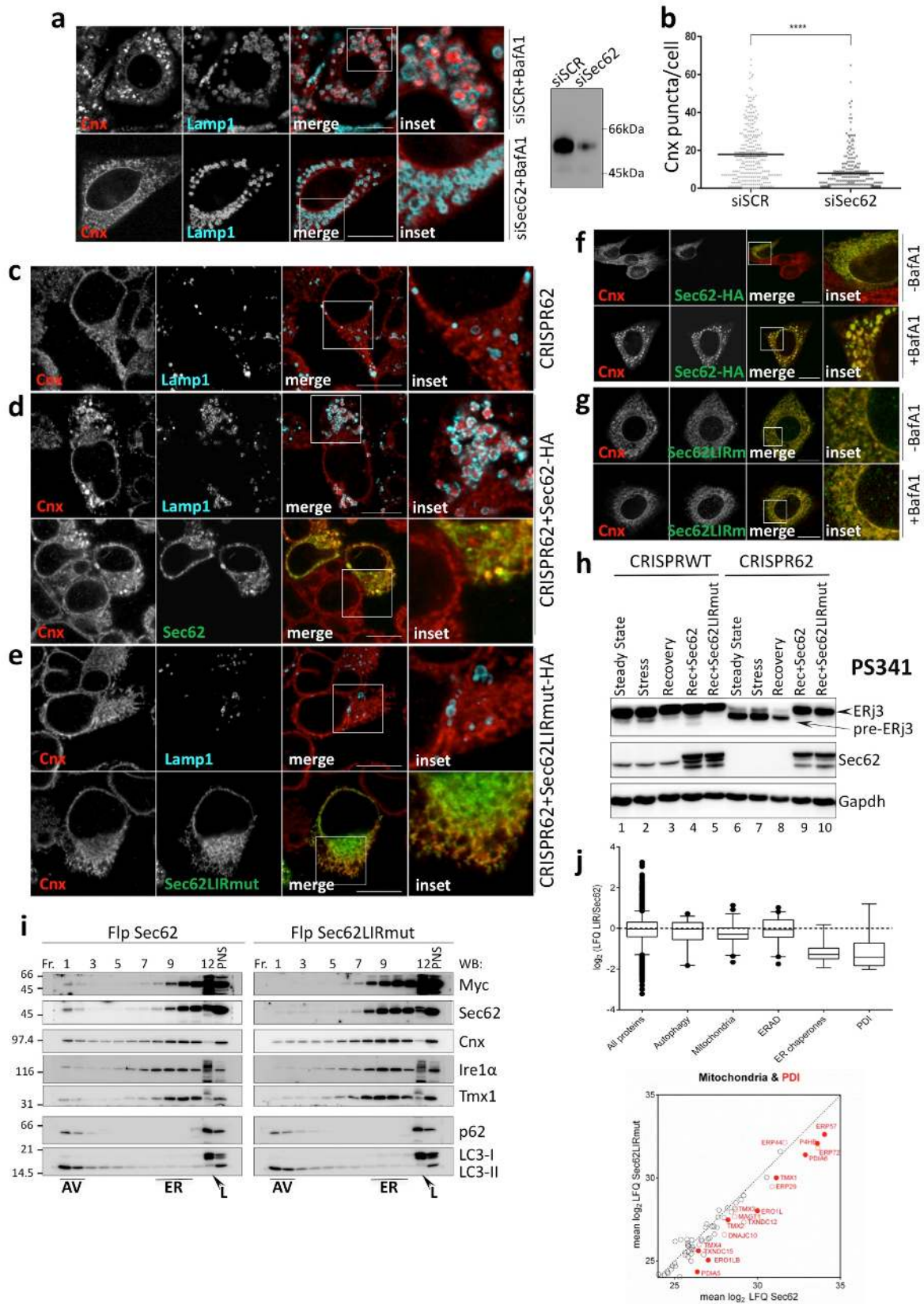
Fig. 4. Sec62-dependent ER-phagy. (a) Sec62 silencing in MEF cells (lower panels) inhibits delivery of Cnx in Lamp1-positive autolysosomes. WB: efficiency of Sec62 silencing. **(b)**

Quantification of (b) as in (Fig. 1i). n = 272 and 229 for siSCR and siSec62, respectively. **Bar=mean. **** p < 0.0001, t-test.** (**c**) In CRISPR62 (Sec62 KO) HEK293 cells, Lamp1-positive vesicles do not contain Cnx upon inhibition of recovery from ER stress by BafA1. (**d**) Same as (c) in CRISPR62 cells after induction of Sec62 expression. Note that ER marker proteins do accumulate in Lamp1-positive vesicles. The lower panels show that Cnx puncta are only present in the two cells expressing Sec62. (**e**) Same as (c) in CRISPR62 cells after induction of Sec62LIRmut expression. The Lamp1-positive vesicles do not contain ER protein markers. (**f**) Recombinant Sec62 induces formation of Cnx (and Sec62)-containing puncta at steady state that accumulate upon lysosomal inactivation (+Baf). (**g**) Same as (f) with the inactive Sec62LIRmut. (**h**) Translocation assay showing compromised ERj3 translocation in CRISPR62 cells (lanes 6-8) and re-established translocation upon Sec62- and Sec62LIRmut-HA expression (lanes 9-10). Translocation efficiency in WT cells is not measurably affected during ER stress (lane 2) or during the recovery from ER stress (lane 3). (**i**) WB analyses of autophagic vesicles (AV) and ER separation in isopycnic gradients of HEK293 cells expressing Myc-Sec62 (left) or -Sec62LIRmut (right). L: loading region. **Extended data Fig. 11c** for Atg7 KO MEF. (**j**) MS-LFQ identifies proteins depleted from AV fraction in cells expressing Sec62LIRmut, whiskers = 5-95 percentile, outliers are aligned (below the dotted line, data from three replicate experiments; **Extended data Fig. 12**). The PDI family members have been selected as example.

Extended data

Materials and Methods

Antibodies, expression plasmids and inhibitors

Antibodies: Cnx (anti C-terminus), Crt and ERp57 were a kind gift from A. Helenius; Cnx (anti N-terminus), anti BiP, Grp94 and ERp72 (Stressgen); Herp (Chondrex and kind gift from K. Kokame); Lamp1 (for IF: 1D4B was deposited to the Developmental Studies Hybridoma Bank (DSHB) by August, J.T., H4A3 by August, J.T. and Hildreth, J.E.K.), for WB: Sigma); Tmx1, HA (for WB) and Myc (Sigma); Actin and HA (for IF, Santa Cruz Biotechnologies); LC3B (Novus and Sigma); GFP (for WB and IP: Abcam, for GFP-LC3 IP: GFP-4C9, DSHB); p62 (MBL); Gapdh (Merck Millipore); Ire1α (Cell Signaling). Sec62, Sec61β, Sec63 and ERj3 are described in [9]. We conclude that the anti-Sec62 antibody is specific for Sec62 under denaturing as well as native conditions since WB and fluorescence microscopy signals were quenched after silencing of the *SEC62* gene [17]. Plasmid encoding GFP-LC3 was a kind gift of N. Mizushima. HRP-conjugated secondary antibodies: anti-mouse (Southern Biotech); anti-rabbit IgG-HRP and anti-rabbit IgG-HRP light chain specific (Jackson Immunoresearch); anti-goat (Santa Cruz Biotechnologies); HRP-ProteinA (Invitrogen); Alexa Fluor-conjugated secondary antibodies (Invitrogen). CPA (Sigma), PS341 (Millennium Pharmaceuticals) or MG132 (Calbiochem), BafA1 (Calbiochem and Sigma), Tun (Sigma), DTT (Roche) and Thaps (Sigma) have been used at final concentrations of 10-50 μM, 10 μM, 50-100 nM, 5 μg/ml, 1mM and 300 nM respectively. DSP (3,3′-Dithiodipropionic acid di(N-hydroxysuccinimide ester, Sigma) at 1 mM.

Cell lines, transient transfection, and RNA interference

Atg7 (WT and KO) and Atg5 (WT and KO) MEF are kind gifts of M. Komatsu and N. Mizushima, Cnx KO MEF of M. Michalak, HeLa cells are from ATCC (CCL-2). Cells were cultured in DMEM supplemented with 10% FBS. Flp-In™ T-REx™ HEK293 inducible cells (Invitrogen) were cultured in DMEM supplemented with 10% FBS, 150 μg/ml hygromycin and 15 μg/ml blasticidin. Cell culture media was supplemented with 100 ng/ml tetracycline (Sigma) for Sec62-myc/Sec62-HA or Sec62LIRmut-myc/ Sec62LIRmut-HA induction. Cells were grown at 37°C and 5% CO_2. All cell lines were tested negative for mycoplasma contamination.

Cells grown at low confluence on Alcian Blue (Sigma)- or poly-L-lysine (Sigma)-coated glass coverslips or finder grids in 3.5 cm, 12 or 6 well tissue culture plates were transfected

with 2 μg, 0.4 μg or 0.8 μg plasmid DNA, respectively, using the jetPrime® reagent (Polyplus transfection). Experiments were performed 17 h after transfection. RNA interferences were performed in MEF plated at 50-60% confluence on Alcian-Blue treated glass coverslips in 3.5 cm dishes. Cells were transfected with siRNA against Sec62 (5'-gaaggaugagaaaucugaatt-3', 100 pmol/dish; Ambion). Cells were fixed 48 h after transfection.

Cell lysis, WB

Cells were harvested and counted before lysis. Cells were washed with phosphate buffered saline (PBS) and then lysed with 2% CHAPS (Anatrace), RIPA buffer (1% TritonX-100, 0.1 % SDS, 0.5% Sodium-deoxycholate in HBS, pH 7.4) or 1% SDS in HEPES-buffered saline, pH 6.8, supplemented with protease inhibitors for 20 min on ice. Post nuclear supernatants (PNS) were collected by centrifugation at 10,000 g for 10 min. Protein concentrations were measured using Coomassie Plus Bradford assay reagent (Thermo Scientific). Samples were denatured and reduced in dithiothreitol (DTT)-containing sample buffer for 10 min at 65 or 5 min at 95 °C and separated by SDS-PAGE. Proteins were transferred to PVDF membranes with the Trans-Blot Turbo Transfer System (Bio-Rad). Membranes were blocked with 10% (w/v) non-fat dry milk (Bio-Rad) and stained with the above mentioned primary antibodies and HRP-conjugated secondary antibodies or ProteinA. Membranes were developed using the Luminata™ Forte ECL detection system (Millipore), signals were detected with the ImageQuant LAS 4000 system (GE Healthcare Life Sciences). Quantifications were performed with Multi Gauge Analysis tool (Fujifilm). For each antigen, the linearity of the detected signal range was ensured with appropriate loading controls.

Cell counting by FACS

Cell number was determined by FACS analysis. ATG7 WT cells were treated for 12 h with 50 μM CPA, 10 μM CPA, 1 mM DTT. At the end of drug treatment and after 12 h of recovery, cells were detached and resuspended in MACS buffer (PBS, 2mM EDTA and 2% FBS) containing CompBeads BD™. Cells were subjected to flow cytometry (BD FACS Canto) and the results were analyzed using FlowJo software.

Inducible, complementable KO cell lines generated with clustered regularly interspaced short palindromic repeats (CRISPR)-Cas9 technology

For construction of the guideRNA-Cas9 plasmid, lentiCRISPRv2-puro system (Addgene 52961) was obtained from Addgene (http://www.addgene.org/). Sequences of the annealed

oligos were obtained from the Cas9 target design tools (www.genome-engineering.org). All protocols and information can be found at the Zhang Lab Gecko website (www.genome-engineering.org/gecko/). The target sequences for guide RNA were synthetized by Microsynth and corresponded to +242 to +261 and +83 to +102 nucleotides from the transcriptional start site of human Sec62 (GI: 1928972) and Sec63 (GI:3978516), respectively. Two annealed oligos (5'-*caccg*ctgtggttgactactgcaac-3', 5'-*aaac*gttgcagtagtcaaccacag*c*-3' for Sec62 and 5'-*caccg*tcccggcgacatactacctc-3', 5'-*aaac*gaggtagtatgtcgccggga*c*-3' for Sec63) were inserted into lentiCRISPRv2-puro vector using the BsmBI restriction site. The plasmid was transfected with Jet Prime (Polyplus) into Flp-In™ T-REx™ HEK293 inducible cells (Invitrogen) according to the manufacturer's instructions to generate CRISPR62 lines. The cells were cultured in DMEM supplemented with 10% FBS, 100 μg/ml zeocin and 15 μg/ml blasticidin. Two days after transfection, the medium was changed with addition of 2 μg/mL puromycin. Puromycin-resistant clones were picked after 10 days. Gene KO was verified by WB. CRISPR62 cells were transfected with either Sec62-HA or Sec62LIRmut-HA plasmids in pcDNA5-FRT/TO under the control of a tetracycline inducible promoter. Cells were cultured in DMEM supplemented with 10% FBS, 150 μg/ml Hygromycin and 15 μg/ml Blasticidin. Inducible Sec62-HA and Sec62LIRmut-HA expression was verified by WB.

Cross-linking

After treatments, cells were washed with PBS and a solution of 1 mM DSP (from a 100 x solution in DMSO) in PBS was added to the dishes. The dishes were incubated with DSP for 30 min at RT. The reaction was stopped with the addition for 15 min at RT of 1 M Tris, pH 7.8, to a final concentration of 20 mM. The dishes were washed with PBS/20 mM NEM and then lysed as described above. SDS-PAGE were run under reducing conditions.

Metabolic labeling, immunoprecipitations

Cells were pulse labeled with 0.1 mCi [^{35}S]-methionine/cysteine mix and chased in DMEM supplemented with 5 mM unlabeled methionine and cysteine. Cells were lysed with 2% CHAPS or RIPA. PNS were pre-cleared with Protein A beads (Sigma, 1:10, w/v swollen in PBS) at 4°C. For immunoprecipitation, the pre-cleared lysate was incubated with Protein A beads (Sigma, 1:10, w/v swollen in PBS) and antibody overnight at 4°C. After washing of the immunoprecipitates with 0.5% CHAPS in HBS or 0.5% Triton X-100, beads were resuspended in sample buffer containing DTT and denatured for 10 min at 65°C or 5 min at

95°C. Samples were subjected to SDS-PAGE. After exposure of the gels to autoradiography films (GE Healthcare, Fuji), films were scanned with the Typhoon™ FLA 9500 (Software Version 1.0). Bands were quantified using the ImageQuant software (Molecular Dynamics, GE Healthcare).

Indirect immunofluorescence (IF) microscopy

MEF plated on Alcian-Blue treated glass coverslips were washed twice in PBS and fixed at room temperature for 20 min with 3.7% formaldehyde diluted in PBS or at -20 degrees for 5 min with 100% methanol. Cells were washed (3 x 5 min) with PBS. The antigen accessibility was improved by 15 min incubation with 0.05% saponin, 10% Goat serum, 10 mM HEPES, 15 mM glycine (PS). Cells were incubated with the primary antibodies diluted 1:100 in PS for 90 min, washed 15 min in PS, then incubated with Alexa Fluor-conjugated secondary antibodies diluted 1:300 in PS for 45 min. Cells were rinsed with PS and water and mounted with Vectashield (Vector Laboratories) supplemented with 4',6-diamidino-2-phenylindole (DAPI).

HEK293 cells plated on Poly-L-lysine treated glass coverslips were washed twice in PBS and fixed at -20 degrees for 5 min with 100% methanol. Cells were washed (3 x 5 min) with PBS. The antigen accessibility was improved by 15 min incubation with 0.1% Triton X-100 in PBS followed by 30 min incubation with 10% Goat serum in PBS (BS). Cells were incubated with the primary antibodies diluted 1:100 in BS for 90 min, washed 15 min in PBS, then incubated with Alexa Fluor-conjugated secondary antibodies diluted 1:300 in BS for 45 min. Cells were rinsed with PBS and water and mounted as previously described.

Confocal pictures were acquired using a Leica TCS SP5 microscope with a 63X/1.4 N.A. objective (Leica HCX PL APO lambda blue 63.0x1.40 OIL UV). Four adjacent fields of view were acquired in each sample, in order to increase the number of cells to be analyzed. The image analysis and processing was performed with FIJI [22]. The quantifications of Cnx (**Fig. 1i, 2i**, **4b** and **Extended data Fig. 4**) and of GFP-LC3:p62 puncta per cell (**Extended data Fig. 11b**) were executed with a custom-developed pipeline in CellProfiler [23] open-source software. The diameter range for detection of the vesicles was set between 0.5 μm and 1.5 μm, according to previous literature observations [24].

Correlative light-electron microscopy (CLEM)

Cells were grown on finder grids and prepared for IF as described above. Z-stacks of cells of interest were taken with the PerkinElmer UltraView ERS confocal microscope. The

coordinates of the cells on the finder grid were determined by bright field microscopy. Cells were fixed in 1% glutaraldehyde in 0.1 M cacodylate buffer (Sigma) and postfixed with 1.5% potassium ferricyanide, 1% OsO4 in 0.1 M cacodylate buffer. Cells were stained with 0.5% uranyl acetate overnight, dehydrated in ethanol and embedded in epon. After backing for 48 h at 60 °C, the resin was released from the glass coverslip by temperature shock in liquid nitrogen. 70-90 nm serial sections were collected on carbon-coated formvar slot grids and imaged with a Zeiss LEO 512 electron microscope. Images were acquired by a 2k x 2k bottom-mounted slow-scan Proscan camera controlled by the EsivisionPro 3.2 software.

Immunogold electron microscopy

Cells were fixed with 3.7 % formaldehyde, followed by washes in PBS and 50 mM glycine. Subsequently, cells were permeabilized with 0.25% saponin, 0.1% BSA and blocked in blocking buffer (0.2% BSA, 5% goat serum, 50 mM NH_4Cl, 0.1% saponin, 20 mM PO_4 buffer, 150 mM NaCl). Staining with primary antibodies and nanogold labeled secondary antibodies was performed in blocking buffer. After washes in PBS, cells were re-fixed in 1% glutaraldehyde and nanogold was enlarged with gold enhancement solution (Nanoprobes, NY, USA) according to manufacturer instructions. Cells were post-fixed with osmium tetroxide, embedded in epon and processed into ultrathin slices. After contrasting with uranyl acetate and lead citrate, sections were analyzed with a Zeiss LEO 512 electron microscope. Images were acquired by a 2k x 2k bottom-mounted slow-scan Proscan camera controlled by the EsivisionPro 3.2 software.

RNA extraction, reverse transcriptase-polymerase chain reaction (RT-PCR) and quantitative real-time PCR (qRT-PCR)

The isolation of total RNA from cells was performed with the GenElute Mammalian Total RNA Miniprep Kit (Sigma) according to the manufacturer's instructions. One to 4 µg of RNA was used for cDNA synthesis with oligo(dT) and the SuperScript II reverse transcriptase (Invitrogen) according to the instructions of the manufacturer. For each qRT-PCR reaction, 10 µl of Power SYBR Green PCR Master Mix (Applied Biosystems or Biotool and 4 µl of milliQ sterile water (3.6 ul and 0.4 reference dye when using Biotool) were added to 5 µl cDNA together with 1 µl of 10 µM forward and reverse primer mix for the transcript of interest. A master mix of SYBR Green and water (mix1) was prepared accordingly to the number of samples and added to the adequate amount of cDNA (mix2). One µl of the primer mix for the genes of interest was pipetted in each well of a 96-Well reaction plate

(MicroAmp Fast Optical 96-Well Reaction Plate with Barcode (0.1 mL), Applied Biosystems) and spun down. Nineteen µl of mix2 was added to each corresponding well and briefly spun down. The plate was sealed, vortexed and centrifuged. Samples were loaded as duplicates. Quantitative Real-Time PCR was performed using a 7900HT Fast Real-Time PCR System. The housekeeping gene Actin was used as reference. Data were analyzed using the SDS 2.2.2 software. Please refer to supplementary table 1 for primer sequences.

Bioinformatics

To determine a possible role of Sec62 as an autophagy adaptor that delivers portions of the ER for lysosomal clearance during ER stress recovery, we performed a bioinformatic search of novel autophagy adaptors using the HHSEARCH method [25]. A multiple alignment of established LC3-interacting regions (LIR [8]) from all phyla was used to construct a LIR-specific Hidden Markov Model (HMM). The LIR-specific HMM was used to screen an extensive database of HMMs covering all sequence families with a human member protein. A HMM derived from metazoan Sec62 sequences **(Extended data Fig. 6a)**, matched the universal LIR-derived HMM with a significance of p=3E-03. An even better significance (p=3E-05) was reached when comparing the conserved Sec62 LIR-candidate in the C-terminal cytosolic domain of Sec62 (-NDFEMIT-, residues 361-367 of human Sec62) with the LIR of the Fam134 protein family [21] **(Extended data Fig. 6b)**. This suggests a resemblance of the two proteins beyond the strict requirements of a functional LIR motif (described by the consensus motif [DE]-[WFY]-x-x-[ILV] embedded within an unstructured sequence context).

SEC62 LIR modeling and docking with LC3

The human LC3B coordinates used for computational docking simulations were obtained from PDBid: 4ZDV [21]. The Sec62 LIR (peptide) was modeled using the available experimental structure of the Fam134B LIR as scaffold. The sequences of the two LIRs differ in 4 amino acids, whose side chains were replaced. Both LC3 and peptide were energy minimized before docking. Computational docking between LC3 and the Sec62 LIR was performed with the FlexPepDock web server [26,27]. LC3 and peptide were initially separated by 10 Å and then docked through 8 cycles of Monte-Carlo search with energy minimization. During each cycle, rigid body perturbation (0.2 Å of translation and 7° of rotation) was followed by side chain repacking and energy minimization. The peptide backbone was similarly perturbed and minimized. Two hundred decoys were created and ranked based on

their Rosetta generic full-atom energy score. The models with best scores were also visually analyzed. Several controls were performed, including different starting positions for the peptide (e.g., rotated by 180°) and docking of the known crystal structure between LC3 and a construct including the Fam134B LIR [21]. Molecular dynamics simulations were performed on the best scoring docking models to evaluate their stability. Standard protocols were used to setup and equilibrate the system prior to simulation with the Gromacs package and the AMBER99SB-ILDN protein force field. Energy minimization, temperature and pressure equilibration of 100 ps were performed before running a molecular dynamics simulation of 100 ns. The trajectory files generated were analyzed after removal of periodic boundary conditions. The model presented in this manuscript shows remarkable stability over time with several intermolecular contacts maintaining the LC3 interaction with the LIR. LIR residues F363 and I366 are deeply inserted in narrow hydrophobic cavities on the LC3 surface. Specific electrostatic interactions are present between residues E364-R70, N361-K51, N361-T50 and M365-K30.

Surface Plasmon Resonance (SPR) and peptide array analyses of Sec62:LC3 binding

Biotinylated peptides Sec62 WT, corresponding to amino acid residues 352-370 of human Sec62 (biotin-KSQHSSGNGNDFEMITKEE) and Sec62 LIR, corresponding to the same residues but with substitution of residues at position 363-366 by four alanines (biotin-KSQHSSGNGNDAAAATKEE) were synthesized on an INTAVIS ResPep SL Synthesizer using the FMOC-solid-phase chemistry. Peptides were purified by HPLC and dissolved in water (1mg/ml). SPR experiments were carried out on a Biacore 2000 system. Identical amounts of WT- or LIR-peptides were coupled to measuring cells of a SA-Chip (Biacore) in 50 mM HEPES/KOH pH 7.3, 150 mM NaCl, 0,05% NP-40 (running buffer) according to the manufacturer´s protocol. LC3 was diluted in running buffer to final concentrations between 0.5 and 16 µM and applied to the flow cells (30 µl/min). Each application was followed by application of running buffer. Response units were recorded as difference between measuring and peptide-free reference cells. Binding parameters were determined with Bia-Evaluation software (4.1.1).

Peptide arrays covering Sec62 WT 259-399 and Sec62 LIR 259-363AAAA366-399 were synthesized on cellulose membranes via carboxy-terminal attachment as described [28]. The peptides consisted of 20 amino acid residues with an overlap of 17 residues with adjacent peptides. LC3 was ^{14}C-labeled by reductive methylation according to established procedures and re-isolated by gel filtration. Membranes were incubated with identical amounts (40 nM)

of ^{14}C-labeld LC3 in binding buffer (50 mM Tris/HCl pH 7.3, 150 mM NaCl, 1% BSA, 0.1% TritonX-100). After washing the membranes three times with binding buffer and drying, the bound proteins were visualized by phosphorimaging. The shown result is representative of three repeats.

Nuclear magnetic resonance (NMR) spectroscopy analysis of Sec62:LC3 association

Solution NMR spectroscopy was used to probe the interaction of unlabeled WT (357-SGNGNDFEMITKEE-370) and mutated LIR (357-SGNGNDAAAATKEE-370) peptides (Genescript) with uniformly ^{15}N labeled LC3, which was prepared in *E. coli* and purified according to standard procedures (GST affinity chromatography and size exclusion following enzymatic cleavage of the fusion tag). [^{15}N,^{1}H]-HSQC spectra were recorded at 298K on a Bruker AVANCE 700 MHz spectrometer equipped with a cryoprobe. Samples were analyzed in 20 mM NaP, 20 mM NaCl, pH 6.8.

Floatation isopycnic OptiPrep^{TM} gradients

Cells were broken by 5 passages through a 25G1 needle. The postnuclear supernatants obtained after 5 min centrifugation at 1500g were loaded below a linear 10–20% OptiPrep^{TM} gradient prepared by mixing a 10% and a 20% (or 10-30%) OptiPrep^{TM} solution (Axis Shield) with a Gradient Master Biocomp^{TM} (angle 80°, speed 20 rev/s, time 90 s). Intracellular organelles were separated by overnight ultracentrifugation at 94,000 g. Fractions were collected from the top and analyzed by WB.

Label free quantitative (MS-LFQ) analyses by mass spectrometry

For quantitative analysis of protein content in the autolysosomal fraction, the upper fraction of the density gradient was subjected to ultracentrifugation at 94,000 g. Membranes were dissolved in 2% SDS sample buffer and separated by 1D mini-PAGE (12% acrylamide) over a distance of 2.0 cm. Entire gel lanes were excised into 5 equal regions from top to bottom and digested with trypsin (Promega) as described [29]. Data-dependent LC-MS/MS analysis of extracted peptide mixtures after digestion was carried out on a Fusion tri-hybrid Orbitrap mass spectrometer (Thermo Fisher Scientific). Data from all five fractions for each sample were pooled and analyzed to identify peptides (at 1% FDR) and obtain Label-Free Quantitation (LFQ) with the software MaxQuant as previously described [5]. Data analysis and annotation was done with the Perseus package [30] and GraphPad Prism. Three replicate experiments were analysed and proteins with statistically significant changes were

determined ($p<0.05$). The MS proteomics data has been deposited to the ProteomeXchange Consortium via the PRIDE [31] partner repository with the dataset identifier PXD003961.

Protein import assay

HeLa cells were cultivated and transfected with either control- or *SEC62*-UTR targeting- (5'-cguaaaguguauucuguactt-3', Qiagen). After 48 h cells were transfected with either control- or *SEC62*-complementation plasmid as previously described [9]. After additional 24 h cells were transfected with an *ERJ3* expression plasmid. After 16 h, PS341 or MG132 were added to a final concentration of 10 µM and the cells were incubated for additional 8 h. Cell lysates were analyzed by SDS-PAGE and WB. Proteins were decorated with ERj3-, Sec62-, and actin-specific antibodies. The primary antibodies were visualized using ECL™ Plex goat-anti-rabbit IgG-Cy5- or ECL™ Plex goat-anti-mouse IgG-Cy3 conjugate, and the Typhoon-Trio imaging system in combination with the ImageQuant TL software 7.0 (GE Healthcare). ERj3 signals were detected using a secondary peroxidase (POD)-coupled anti-rabbit antibody (Sigma) and ECL (GE Healthcare), visualized with a Fusion SL (peqlab) luminescence imaging system. Silencing- and complementation-efficiencies are given together with standard errors of the mean in percent of control siRNA- and plasmid-treated cells and normalized to ß-Actin. We note that the precursor of ERj3 (pERj3) is seen only upon proteasomal inhibition with PS341 or MG132 and that mature ERj3 protein corresponds to precursor, which had been processed by signal peptidase and N-glycosylated by oligosaccharyl transferase. Transport-efficiencies were calculated as ERj3 in percentage of ERj3 plus ERj3 precursor.

Extended data Fig. 1. Toxicity and reversibility of ER stress induction: selection of CPA as ER stress inducer to investigate mechanisms of recovery from ER stress.

(**a**) MEF were treated for 12 h with DMSO (mock), 10 µM CPA (reversible SERCA inhibitor), 300 nM thapsigargin (Thaps, irreversible SERCA inhibitor) or 5 µg/ml tunicamycin (Tun, irreversible GPT inhibitor). Cells were harvested and the number of viable cells was assessed at the end of the stress phase by Trypan Blue staining and subsequent cell counting. In contrast to CPA, Thaps and Tun cause cell death. Their toxicity and their irreversibility that would require new synthesis of their target enzymes to recover from stress after their wash out led to their exclusion from our experiments.

(**b**) Dithiothreitol (DTT) induces ER stress by modifying redox homeostasis. At 1 mM, DTT caused a milder stress in MEF compared to non-toxic concentrations of CPA as determined by lower induction of BiP transcription.

(**c**) Even though DTT was not further considered for our in-depth analysis of mechanisms operating during recovery from ER stress, tests performed with this compound revealed that, like CPA, the wash out at the end of the stress phase was followed by rapid return of BiP transcripts at or below their pre-stress, physiologic levels as determined by qPCR.

(**d**) Like CPA, upon DTT wash out, excess ER chaperones did accumulate in Lamp1-positive autolysosomes in cells exposed to the lysosomal inhibitor BafA1.

Extended data Fig. 2.

(**a**) Transcripts for unspliced and spliced XBP1 in mock-treated cells and in cells exposed to 10 μM CPA-induced ER stress. (**b**) Incorporation of ^{35}S-radiolabeled amino acids (2 h pulse with ^{35}S-methionine and -cysteine) in total MEF proteome after 8 h of Mock- or 10 μM CPA-treatment. TCE, total cell extract. (**c**) Same as (b) for the incorporation of ^{35}S-radiolabeled amino acids in the ER marker proteins Cnx, Grp94 and BiP as assessed by autoradiography of the respective immunoprecipitates. (**d**) Quantification of (b) and (c). (**e**) For Herp, which is characterized by a fast recovery rate, which is not inhibited by BafA1 (**Fig. 1c-f**), return to pre-stress levels upon CPA wash out is delayed by PS341, a proteasomal inhibitor. The protein level was analyzed by WB. Shown is the mean +/- SEM of three independent experiments. (**f**) For the model ER proteins with slow recovery rate Cnx and BiP return to pre-stress levels is delayed by BafA1. Return of Herp to pre-stress levels is unaffected by BafA1 (as also shown in **Fig. 1e,f**). (**g**) In Atg7 KO MEF lacking autophagy, the return of the select ER protein marker BiP to pre-stress levels is blocked. Return of Herp is unaffected.

Extended data Fig. 3:

(**a**) Cnx accumulates in autolysosomes displaying GFP-Rab7 and Lamp1 (also refer to **Fig. 1g, 2a, 4b, e, g**) upon inhibition of recovery from ER stress with BafA1 (+BafA1).

(**b**) Same as (a) for Sec62 (also refer to **Fig. 2b, 4e, g**).

(**c**) The soluble ER proteins markers (Crt in this figure) do also accumulate in autolysosomes displaying Lamp1 at the limiting membrane upon inhibition of ER stress recovery with BafA1 (+BafA1).

Extended data Fig. 4: Reversibility of the recovery block obtained by cell exposure to the lysosomotropic drug BafA1. (**a**) After the CPA-induced stress, MEF were grown in the presence of BafA1 for 12 h and analyzed in IF (upper panels) or analyzed in IF 4 h after BafA1 wash out (lower panels). (**b**) Quantification of the Cnx-containing puncta in the upper and lower panels. Two independent experiments, n = 206 and 112 for +BafA1 and BafA1 wash out, respectively. Bar = average. **** $p < 0.0001$, t-test.

Extended data Fig. 5: Analysis of ER protein markers accumulation in cytosolic puncta.

(**a**) Sec62 accumulation in autolysosomes displaying GFP-Rab7 at the limiting membrane of Cnx KO MEF. Cnx is not required for delivery of ER protein markers to autolysosomes during recovery from CPA-induced ER stress.

(**b**) Controls of GFP-LC3 and Lamp1 co-localizations in autolysosomes accumulating with their content upon inhibition of ER stress recovery with BafA1.

Extended data Fig. 6: The LIR of Sec62: sequence conservation and *in vitro* association with LC3B.

(**a**) Amino acid conservation of Sec62 among species. The LIR in the cytosolic C-terminus of Sec62 is in red.

(**b**) Comparison of the LIR of Sec62 and Fam134. Residue numbers are given.

(**c**) Comparison by peptide array and phosphorimaging of ^{14}C-LC3 binding to 41 oligopeptides scanning amino acid residues 259-399 from the cytosolic C-terminal domain of human Sec62. LC3 binds to peptides 32-35 (they contain the -FEMI- sequence) and not to corresponding mutant peptides 32'-35' (where the FEMI sequence has been mutated to -AAAA-). The sequence of peptide 33 (binding) and 33' (no binding) are highlighted in red and blue, respectively. Note that LC3 weakly binds to peptides 9 and 10.

Extended data Fig. 7: The LIR of Sec62: *in vivo* association with LC3

(**a**) Endogenous Sec62-containing complexes stabilized with the chemical cross linker DSP have been immunoisolated from lysates of MEF non-treated (-, lane 4) or treated with BafA1 (+, lane 5). Immunocomplexes have been separated in reducing SDS-PAGE, transferred on PVDF membrane, which was then revealed with anti Sec62 (upper panel) or anti LC3 antibodies. BafA1 stabilized endogenous Sec62:LC3-II complexes. *, non-specific bands. PAB: control of proteinA beads without antibody; Ab: control of antibody without PAB.

(**b**) MEF have been mock-transfected (pcDNA3.1, lane 2), transfected for expression of GFP-LC3 and Sec62 (lane 3) or for expression of GFP-LC3 and Sec62LIRmut (lane 4). Complexes containing ectopic GFP-LC3 were stabilized with the chemical cross linker DSP, immunoisolated with GFP-specific antibodies, separated in reducing SDS-PAGE, transferred on PVDF membrane, which was then revealed with anti HA antibodies. Sec62, but not Sec62LIRmut associates with recombinant GFP-LC3 (lane 3).

(**c**) Same as (a) in CRISPRWT (right panel, lane 3) CRISPR62 (right panel, lanes 4 and 6), CRISPR62 induced with Tet for expression of Sec62 (right panel, lane 5) or of Sec62LIRmut (lane 7), CRISPR63 and CRISPR63 induced with Tet for expression of Sec63. To be noted that endogenous (lane 3) and ectopically expressed Sec62 (lane 5) do associate with LC3-II. Ectopically expressed Sec62LIRmut (lane 7) does not. Importantly, endogenous Sec62 does associate with endogenous LC3-II in cells lacking Sec63 (lane 8). Ectopic expression of Sec63 reduces the association of endogenous Sec62 and LC3-II (as observed in three independent experiments) supporting a model, where Sec62 intervention during post-translational protein translocation (requires Sec63) and during recovery from ER stress (does not require Sec63) are mechanistically distinct events. Panels on the left are controls of protein KO (lanes 2 and 4) and of ectopic Sec62/LIR (lanes 3 and 5) and Sec63 expression (lane 7) expression.

Extended data Fig. 8: Generation of CRISPR62 and CRISPR63 cell lines and characterization of ER stress recovery.

(**a**) Control of Sec62 (upper panel) and Sec63 (lower panel) KO in HEK293 cells inducible for Sec62 expression. *, non-specific cross-reacting bands.

(**b**) Induction of Sec62-HA or Sec62LIRmut-HA in CRISPR62 cells exposed to increasing (0-150 ng/ml) Tetracycline concentrations.

(**c**) CRISPR62 HEK293 cells as well as the same cells upon induction of Sec62 (upper panel) or Sec62LIRmut expression (lower panel) for 17 and 41 h do not activate the UPR. As positive control, cell exposure to CPA (30 µM) or tunicamycin (5 µg/ml) induces an UPR.

(**d**) Reversibility of the transcriptional UPR induced upon cell exposure to 30 µM CPA in the absence or presence of 100 nM BafA1. Note that the presence of BafA1 does not affect the rate of BiP and sXbp1 transcripts reduction upon CPA wash out.

(**e**) Deletion of Sec62 (CRISPR62 HEK293 cells) prevents delivery of ER marker proteins to Lamp1-positive autolysosomes during recovery from ER stress (upper panel). Deletion of Sec63 leads to delivery of ER protein markers to Lamp1-positive autolysosomes even at steady state (CRISPR63, steady state) and it does not interfere with delivery of ER protein markers to Lamp1-positive autolysosomes during recovery from ER stress (CRISPR63, Recovery).

(**f**) Comparison of BiP decay in CRISPRWT *vs.* CRISPR62 HEK 293 cells reveals that the KO of Sec62 inhibits return to pre-stress level after conclusion of the ER stress upon CPA wash out. The return of Herp, which is regulated by the 26S proteasome (**Extended data Fig. 2e**), is not affected in Sec62 KO cells.

(**g**) Tetracycline-inducible HEK293 cells expressing Sec62 or Sec62LIRmut. Upper panel, r: Sec62-myc (lanes 2-4) or Sec62LIRmut-myc (lanes 6-8). e: endogenous Sec62. Middle, Cnx. Lower, Gapdh. Variations of endogenous Sec62 and Cnx are given in % of their content before Sec62 or Sec62LIRmut induction. Note that induction of Sec62 at steady state reduces the intracellular content of endogenous Se62 and Cnx. This is consistent with an enhanced delivery of these ER marker proteins to autolysosomes for clearance. The expression of Sec62LIRmut rises the content of endogenous Sec62 and, to a much lower extent, if at all, of Cnx.

Extended data Fig. 9: The cytosolic LIR motif of Sec62 is required and sufficient for delivery of ER portions to autolysosomes.

(**a**) At steady state, Cnx is delivered to Lamp1-positive autolysosomes in cells expressing ER membrane-associated GFP displaying the 145 C-terminal residues of the cytosolic tail of Sec62 (GFP$_{TM}$62) containing the LIR. MEF are shown.

(**b**) Cnx is not delivered to autolysosomes in cells expressing GFP$_{TM}$62LIRmut.

(**c**) Same as (a) for Crt. Note that the inset in the panel +BafA1 highlights the presence of Crt in Lamp1-positive autolysosomes in the upper cell expressing GFPTM62 and the absence of Crt in Lamp1-positive autolysosome in the non transfected cells.

(**d**) Same as (b) for Crt.

Extended data Fig. 10: ERj3 depends on Sec62:Sec63 for post-translational translocation in the mammalian ER. In a complementation or rescue assay, the Sec62 and Sec62LIRmut equally support ERj3 translocation into the ER of Sec62 silenced MEF (please also refer to **Fig. 4h**). Expression (Sec62) and transport (ERj3) efficiencies were calculated as described in the Methods section. Averaged efficiencies are given together with standard errors of the mean for four repeats. We note that SEC62 plasmids (lanes 2-4 and 6-8) lack the untranslated region (UTR) of endogenous mRNA and, therefore, are resistant to UTR-targeting siRNA, and that a similar inhibitory effect of Sec62 depletion (lane 1 versus 5) is seen with a siRNA, which targets the SEC62 coding region (data not shown) and in CRISPR62 cells (**Fig. 4h**).

Extended data Fig. 11: Separation of AV and ER in isopycnic density gradients

(**a**) Schematic representation of the experiments. At the end of the ultracentrifugation, AV float at the top of the density gradient, the ER has higher density (**Fig. 4i**).

(**b**) The number of LC3-GFP:p62 puncta has been counted in cells with normal (siSCR, n=394 cells) and reduced level of Sec62 (siSec62, n=316 cells). t test; ns: not significant difference.

(**c**) Extracts of Atg7 KO cells were prepared and loaded at the bottom of an isopycnic density gradient (as in **Fig. 4i** and Methods). Fractions floating at the top of the gradient (AV) and fractions containing the ER were separated in SDS-PAGE and probed for the presence of Cnx, Sec62 and LC3.

Extended data Fig. 12:

Mass spectrometry-based label-free quantitation (MS-LFQ) of proteins in autophagic vesicles (AV) enriched from HEK293 cells expressing Sec62 vs. Sec62LIRmut. LFQ values are the mean of three replicates and are expressed as log(2). Proteins depleted in Sec62LIRmut AV are on the right side (below) of the diagonal. Full circles : proteins with statistically significant difference (T-test p<0.05). Red circles : PDI proteins. Assignment to families or functional classes is based on manual curation. The MS proteomics data has been deposited to the ProteomeXchange Consortium via the PRIDE [31] partner repository with the dataset identifier PXD003961.

Extended data Table 1: Sequences of primers used for qPCR

Gene	Primer sequence forward 5'-3'	Primer sequence reverse 5'-3'
Mouse		
Actin	CTTTCTGGGTATGGAATCCT	GGAGCAATGATCTTGATCTT
BiP	GAGTTCTTCAATGGCAAGGA	CCAGTCAGATCAAATGTACCC
Cnx	CCAAGCATCATGCCATCTCT	GCCTTTCATCCCAATCTTCA
Crt	CCTGGCACCAAGAAGGTT	CCATCTCTTCATCCCAGTCCT
Edem1	AGTCAAATGTGGATATGCTACGC	ACAGATATGATATGGCCCTCAGT
ERp57	TCAAGGGTTTTCCTACCATCTACTTC	CATTTAATTCACGGCCACCTTCATAC
ERp72	CATCGCCAAGATGGATGCTACTG	ATAGATGGTAGGGAAGCCCTCC
Grp94	CTGGGTCAAGCAGAAAGGAG	TGCCAGACCATCCATACTGA
Herp	GCAGTTGGAGTGTGAGTCG	TCTGTGGATTCAGCACCCTTT
sXbp1	CTGAGTCCGCAGCAGGTG	TGGCTGGATGAAAGCAGATT
Human		
Actin	CTTCCTGGGCATGGAGTCCT	GGAGCAATGATCTTGATCTT
BiP	GAGTTCTTCAATGGCAAGGA	CCAGTCAGATCAAATGTACCC
sXbp1	CTGAGTCCGCAGCAGGTG	TGGCTGGATGAAAGCAGATT